Alfvén wave current drive in the Phaedrus-T tokamak*

T. Intrator,† P. Probert, S. Wukitch, M. Vukovic, D. Brouchous, D. Diebold, R. Breun, M. Doczy, D. Edgell, A. Elfimov, N. Hershkowitz, M. Kishinevsky, C. Litwin, P. Moroz, P. Nonn, and G. Winz

Department of Nuclear Engineering and Engineering Physics, University of Wisconsin, Madison, Wisconsin 53706-1687

(Received 14 November 1994; accepted 8 February 1995)

The first experimental evidence of Alfvén Wave Current Drive (AWCD) in a tokamak is shown. In a low-density experiment, an estimated 20–35 kA out of 65 kA total current, or 30%–55% of the total current has been driven. The estimated efficiency for current driven per unit RF input power is approximately $I_{CD}/P_{RF}\approx 0.2$ A/W, which is near the predicted efficiency, and corresponds to the commonly used figure of merit, $n_e R_0 I_{CD}/P_{RF}\approx 0.4\times 10^{18}$ A m^{-2} W^{-1}, where n_e is plasma density and R_0 is the major radius. The significant 30%–40% drop in loop voltage observed cannot be explained by any plausible increase in electron temperature T_e, or decrease in inductive plasma energy, or changes in plasma resistivity. Independently measured loop voltage, T_e, effective ionic charge Z_{eff}, and plasma inductance and resistance are all consistent with this conclusion. © *1995 American Institute of Physics.*

I. INTRODUCTION

Even though tokamaks are usually operated as pulsed devices, they will not be attractive as controlled fusion power reactors until some way of continuously driving the plasma current[1] is practical. Typically the pulsed toroidal tokamak plasma current is driven by an inductively coupled Ohmic transformer. A pulsed design with its attendant thermal and mechanical stresses would not be compatible with continuous reactor power output.

Of the several noninductive current drive schemes that have been tried, Lower Hybrid Current Drive (LHCD) has been the most successful so far in tokamaks[2–5] including synergism (LHCD+FWCD)[6] with fast magnetosonic waves (FWCD),[7] and current drive from electron cyclotron waves (ECCD),[8] and neutral beams (NBCD).[9] We show in this paper evidence that Alfvén Wave Current Drive (AWCD) of 20–35 kA out of 65 kA or 30%–55% of the total plasma current has been achieved in a low-density plasma in the Phaedrus-T tokamak. The primary evidence is a large (30%–40%) drop in plasma loop voltage, while the Ohmic resistance rises during the RF pulse. Measurements of Thomson Scattering electron temperature, effective ionic charge Z_{eff} from visible bremsstrahlung emission, plasma inductance from a plasma termination experiment, and estimated overall power balance all support this conclusion. The AWCD increases the internal inductance by approximately 4%–8%, and we estimate that 3% of the RF power has been converted to poloidal field energy.

There are numerous theoretical predictions that in an inhomogeneous magnetized plasma Alfvén waves can have a resonance.[10] Electron heating by Alfvén waves at a spatially localized surface,[11,12] can then occur, e.g., in the solar corona[13] or during the formation of auroral arcs[14] or in tokamaks.[15] In a tokamak, electron heating[16–18] and current drive[19] for frequencies below the ion gyrofrequency $\omega<\omega_{ci}$ (Alfvén regime) is accessible using the Ion Cyclotron Range of Frequencies (ICRF) fast wave antenna heating systems. This scenario takes advantage of mode conversion from antenna launched fast magnetosonic (FM) wave fields.[16,20,21] The FM wave is a compressional wave polarized in the right-hand circular or electron diamagnetic direction, which can propagate perpendicular, as well as parallel to the magnetic field lines. The Phaedrus-T antenna launches predominantly FM waves.

There are many reasons why it makes sense to investigate AWCD. Low wave phase speed (v_ϕ) Current Drive (CD) is attractive because less power is required to push a slow electron than a fast one. These waves resonate near the electron thermal speed v_e and Landau damp on the large bulk electron population. There is no high-density cutoff, which is an advantage over LHCD. In fact, higher densities will lead to lower Alfvén speeds, hence a lower ratio v_ϕ/v_e and therefore higher current drive efficiency. Spatially localized waves[22,23] and mode conversion[24] have been observed in several Alfvén wave experiments, and some success with AWCD was observed in the RO stellarator.[25] If this local RF power deposition scales to larger devices, it should be possible to tailor profiles of plasma current I_p and electron temperature T_e. Radio frequency (RF) hardware in this frequency range of 1–20 MHz is reliable and large transmitter power is inexpensive. For electron heating or CD (even with FM waves), ion resonances and undesirable ion heating can be avoided, provided $\omega<\omega_{ci}$. The Alfvén regime is therefore being considered for the International Thermonuclear Experimental Reactor (ITER).[26]

Historically AWCD has not gotten much experimental attention because mirror electron trapping[27] is theoretically predicted for $v_\phi\approx v_e$ in tokamaks. If one assumes that particles orbiting along helical magnetic field B lines conserve magnetic moment $W_\perp/B$, then those particles traveling "up" the magnetic field gradient will increase their perpendicular kinetic energy $W_\perp$ at the expense of parallel energy $W_\parallel$. Since the toroidal magnetic field increases at small major

*Paper 8IA2, Bull. Am. Phys. Soc. **39**, 1720 (1994).
†Invited speaker.

radius, particles with relatively small $W_\parallel$ compared with $W_\perp$ tend to reflect near the high-field side and be "trapped" on banana orbits. Since low phase speed current drive affects these slower electrons, and if the "passing" population is thus reduced, then trapping may reduce or eliminate CD. The trapped fraction of electrons is proportional to the ratio of banana bounce frequency ω_b to (Coulomb) collision detrapping frequency ν_c. One potential pitfall of low phase speed CD is that thermal electron heating from waves with $v_\phi \approx v_e$ would tend to increase v_e, decrease ν_c, and exacerbate these trapping problems. Others conjecture trapping is not a problem.[28,29] In any case, this issue has never been experimentally tested. The pioneering Alfvén wave experiments on the Tokamak à Chauffement Alfvén (TCA)[30] that could have addressed this issue were plagued by an uncontrollable density rise that greatly complicated their experiments. In Phaedrus-T the use of insulating antenna limiters solves this problem.[31]

There is a significant database for Alfvén wave and Alfvén heating experiments and theoretical work done at TCA, and the somewhat smaller Torus of the University of Sydney (TORTUS)[32] tokamak. Alfvén heating was observed on stellarators such as Proto-Cleo[33] and Heliotron-D,[34] and AWCD was apparently observed in the RO-5 stellarator.[35] In small tokamaks such as Tokapole,[23] *in situ* measurements of Alfvén wave fields were carried out, and evidence of discrete Alfvén eigenmodes were observed in the Texas Experimental Tokamak PRETEXT.[36] In linear solenoidal devices with a hot cathode source,[37] an arc jet[38] device, theta pinch,[39] and tandem mirrors,[40,41] measurements of Alfvén wave field structures have been made.

The organization of this paper is as follows. In the Introduction we outline the significance of Alfvén Wave Current Drive in tokamaks and this proof of principle experiment. Section II includes an experimental description, Sec. III a definition of current drive efficiency, in Sec. IV we present the experimental evidence for AWCD, in Sec. V we describe measurements of plasma inductance and resistance with a plasma turn-off experiment, in Sec. VI we estimates the fraction of AWCD, in Sec. VII we outline an approximate power balance, in Sec. VIII we describe the relevant time scales, and Sec. IX shows a relationship between the optimal wave number and plasma density or ion skin depth, with conclusions offered in Sec. X.

II. EXPERIMENT DESCRIPTION

Phaedrus-T is a medium-sized tokamak[42] with a major radius $R_0=0.93$ cm and minor radius $a=0.25$ m, with a peak central electron temperature of $T_e(0)=300$–500 eV. For this experiment we operated the device with a nominal hydrogen gas fill, plasma current of $I_p=65$ kA, edge safety factor $q(a)\approx 3.5$, line-averaged density $\langle n_e\rangle \approx 2.3\times 10^{18}$ m^{-3}, toroidal magnetic field of $B_0=0.67$ T on axis. Boronization with Trimethyl Boron[43] and time programmable gas puffing was critical to wall conditioning and control of RF-induced gas reflux.

A two strap fast wave antenna array[30] consisting of two low-field side toroidally spaced poloidal current straps subtending 60° of a poloidal arc was used to drive wave fields, with phase speed $v_\phi=\omega/k_z$, corresponding to an electron thermal speed where $T_e\approx 50$–150 eV, or a parallel index of refraction $N_\parallel \approx ck_z/\omega \approx 70$. There is no Faraday shield,[30] and vacuum loading, or Ohmic dissipation in the antenna and due to image currents in the tokamak walls, accounts for approximately 30% of the total 300–400 kW available from the transmitter. Operation was at a frequency of 6.53 and 7.00 MHz or $\omega/\omega_{cH}\approx 0.7$ on axis. Two straps were spaced at 15 cm and phased at $[0,\pi/2]$, corresponding to traveling wave launch parallel to the direction of the electron current. The measured peak of the vacuum k_z spectrum was at $k_z\approx 0.1$ cm^{-1}, and the poloidal mode spectrum includes $|m|\leq 2$. The ICRF antennas at the edge launch evanescent Fast Magnetosonic (FM) fields that extend into the plasma, approximately as $e^{-k_z r}$. In the usual cylinder model picture of the Alfvén resonance, the density and B_θ gradients affect the local Alfvén speed $v_A(r)$ and the Alfvén frequency,

$$\omega_A^2(r)\approx \frac{[n+m/q(r)]^2}{R^2}\left(1-\frac{\omega^2}{\omega_{ci}^2}\right)v_A^2(r), \tag{1}$$

where the toroidal and azimuthal mode numbers are n, m, the ion cyclotron frequency is $\omega_{ci}(R=R_0)$, and the safety factor is $q(r)$. If $v_\phi < v_e$, theory predicts[44,31,29,45] mode conversion to a Kinetic Alfvén Wave (KAW), with substantial Landau damping onto the electrons. A directional wave launch would thus induce more AWCD, and a nondirectional launch would heat the electrons.

III. CURRENT DRIVE EFFICIENCY

If RF power density is applied to a plasma, the portion of it dissipated by collisions is

$$\Delta P_D = n m_e v_\parallel \, \Delta v_\parallel \, \nu_{\rm coll}(v_\parallel), \tag{2}$$

where the collisions mediate a transfer of momentum between RF waves and the electrons. In this case the Coulomb collision frequency scales as

$$\nu_{\rm coll}(v_\parallel)\approx \frac{\ln\Lambda}{2\pi}\frac{\omega_{pe}^4}{n_e v^3}\approx n_e(v_\parallel^2+v_\perp^2)^{-3/2}. \tag{3}$$

The resulting plasma current from the momentum transfer is

$$\Delta J = n_e e \, \Delta v_\parallel. \tag{4}$$

A suitable figure of merit is the current density driven per unit RF power density,[1,46,47]

$$\eta\left(\frac{\rm m}{\rm V}\right)=\frac{\Delta J}{\Delta P_D}=\frac{e}{m_e}\frac{1}{v_\parallel \nu_{\rm coll}(v_\parallel)}. \tag{5}$$

A dimensionless efficiency quantity $\tilde{\eta}$ (Fisch–Karney)[1] calculated using a Fokker–Planck collision operator is given by

$$\tilde{\eta}=\frac{\tilde{J}}{\tilde{P}_D}=\frac{\Delta J/e n_e v_e}{\Delta P_D/n_e m v_e^2 \nu_{\rm coll}(v_e)}. \tag{6}$$

In Fig. 1 we plot $\tilde{\eta}$ vs v_ϕ/v_e from the original Fisch–Karney[1] calculations, where $\tilde{\eta}$ (Fisch–Karney) is given on the left-hand vertical axis. This axis scale coincides with $2\times\tilde{\eta}$ (Ehst–Karney) from the formulation of Ehst–Karney,[48] which accounts for a more realistic $Z_{\rm eff}>1$, where the respective $\tilde{\eta}$ for Landau damping (labeled LD) and Transit Time

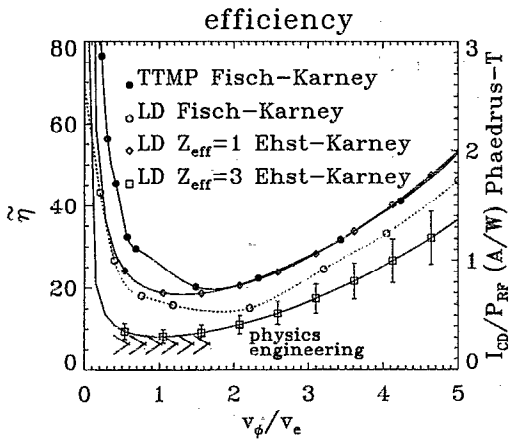

FIG. 1. Plot of normalized current drive efficiency Here $\tilde{\eta}_{CD}$ defined in Eq. (6) versus v_ϕ/v_e, with efficiency I_{CD}/P_{RF} in A/W on the right-hand scale. The upper and lower experimental data regions indicated by the diagonal hatched lines are, respectively $(I_{CD}/P_{RF})^{phy}$ and $(I_{CD}/P_{RF})^{eng}$. Error bars for Z_{eff}=3 follow from the ±20% uncertainty in T_e. The figure of merit, γ_{CD}(A W^{-1} m^{-2}) can be calculated from Eq. (8) using $\langle n_e\rangle=2.3\times10^{18}$ m^{-3} and R_0=0.93 m.

Magnetic Pumping (labeled TTMP) damping mechanisms are displayed. The damping is expected to be mostly LD with some fraction of TTMP. Apparently $\tilde{\eta}$ (Ehst–Karney)[48] is normalized, such that it corresponds to $\tilde{\eta}/2$ (Fisch–Karney).[1] The right-hand vertical axis shows the efficiency I_{CD}/P_{RF}(A/W)$=\eta\pi a^2/(2\pi R_0\pi a^2)$ rescaled to our experimental parameters, where

$$\eta\left(\frac{\mathrm{m}}{\mathrm{V}}\right)=1.92\times10^{19}\,\frac{\tilde{\eta}(\text{Fisch–Karney})T_e(\mathrm{keV})}{n_e(m^{-3})\ln(\Lambda)}. \qquad (7)$$

For comparison with other experiments, a standard figure of merit is

$$\gamma_{CD}(\mathrm{A\,m^{-2}\,W^{-1}})=\langle n_e\rangle R_0 I_{CD}/P_{RF}. \qquad (8)$$

For low phase speed $v_\phi<v_e$, so that the collisionality $\nu_{coll}(v_\parallel)\approx$const, and therefore the efficiency $\tilde{\eta}\approx1/v_\parallel$ gets large, as seen in Fig. 1 for $v_\phi/v_e\ll1$. In this regime the large ratio of momentum to energy content[49,1] (k_z/ω) would yield high efficiency if trapping were not a problem.[50] The cross-hatched regions near $v_\phi/v_e\approx1$ correspond to the error bar limited region, where our AWCD data is estimated to lie on this plot. The lower value is an engineering efficiency based on the total P_{RF} that gets into the core, the larger value is a physics efficiency that is based only on the estimated P_{RF} that does the AWCD, and not the portion that does the electron heating, as outlined in Sec. VII. The experimental data lie near $\tilde{\eta}$ the predicted efficiency. This experimental data corresponds to an engineering $\gamma_{CD}\approx0.34$–0.47×10^{18} A W^{-1} m^{-2}, and a physics $\gamma_{CD}\approx0.68$–0.92×10^{18} A W^{-1} m^{-2}.

Several competing considerations constrained these initial experiments to fall near the minimum of the efficiency curve in Fig. 1. Frequency and wave number determine the experimentally available wave phase speeds v_ϕ, which in these data fall near $v_\phi\approx v_e$. Frequency was chosen so that the hydrogen (nominal fill gas) and deuterium (or fully stripped impurity) cyclotron gyroresonances do not interfere with the interpretation of the experiment, and fall, respectively, outside the low-field side antenna limiter and near the high-field side limiter. The wave number spectrum is constrained to $k_z\approx0.05$–0.15 cm^{-1} when our antenna array is phased for a traveling wave launch. Larger k_z (smaller v_ϕ) might result in less FM wave access to the core because of the radial edge evanescence mentioned in Sec. II, or miss the Alfvén resonance altogether. On the other hand, one might exploit more extensive antenna arrays, or the radial upshift for inward propagating k_z,[51] or heavier ion species with lower Alfvén speeds (e.g., He^3) or Alfvén ion–ion hybrid scenarios to gain access to more efficient AWCD regimes.

IV. EXPERIMENTAL EVIDENCE FOR AWCD

Since the CD efficiency η favors low density, we chose a low-density experiment where $n_e(0)\approx3\times10^{18}$ m^{-3}, compared with the typical operation at $n_e(0)\approx2\times10^{19}$ m^{-3}, to show that a substantial fraction (20–40 kA) out of the total tokamak plasma current (65 kA) could be driven. At low density there is less collisional relaxation, therefore, more momentum available per particle. AWCD is not measured directly, but inferred from a drop in loop voltage not explainable by any measurable changes in plasma conductivity calculated from Thomson scattering T_e, visible bremsstrahlung emission Z_{eff} line density n_e, launch RF power, or inductance inferred from the plasma position and a plasma termination experiment.

A typical tokamak shot is summarized in Fig. 2, where approximately 200 kW of ICRF coupled power (vacuum loading is already subtracted out) gates on with approximately four times the Ohmic power during time 110–160 ms. The plasma current is maintained by a feedback system, but the loop voltage V_{loop} drops promptly some 30%–40%, and drifts up slowly, while the RF power droops by 30%, and RF-generated impurities increase the plasma resistivity. During the RF pulse, the plasma current I_p changes less than ±0.3%, the interferometer line density changes by less than ±5%, and the plasma position as measured by sine–cosine coils is stable to within ±0.2 cm or 0.2%. The total plasma emission increases by 40%–70%, as shown by the pyrobolometer signal that views the entire poloidal section, and the Soft X-Ray (SXR) signal that increases. Visible bremsstrahlung radiation ϵ_{VB} from which we infer Z_{eff} is shown here to increase 40%–70%. In Fig. 3, the radial electron temperature profile as measured in a vertical chord by Thomson scattering is shown. Within the error bars of ±20%, $T_e(r)$ does not change during the RF pulse.

The AWCD drop in loop volts cannot be due to a decrease in plasma resistivity. The Z_{eff} radial profile data in Fig. 4 show that plasma resistivity *increases* during RF. Visible bremsstrahlung radiation emissivity[52] $\epsilon_{VB}\approx Z_{eff}n_e^2T_e^{-1/2}$ is measured, and Abel inverted $Z_{eff}(r)$ increases by 40%–70% during the RF pulse. This would correspond to either a decrease in T_e or an increase in density, but these are measured to be constant. In Fig. 4, the Z_{eff} profile does not change much, but increases from $Z_{eff}\approx1.5$ some 10 ms before RF begins, to $Z_{eff}\approx2.5$ some 10 ms after the RF pulse begins. As

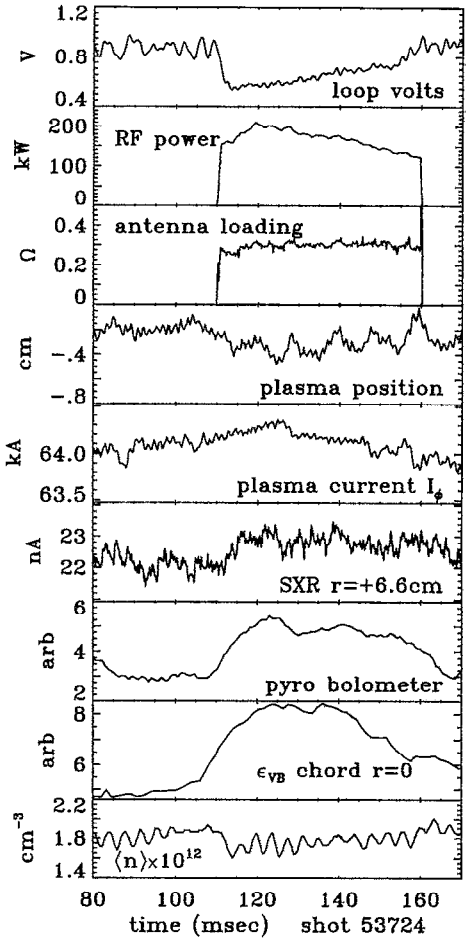

FIG. 2. Typical tokamak shot showing AWCD with diagnostics from top to bottom, loop voltage (V), RF power excluding vacuum loading (kW), antenna plasma loading excluding vacuum loading (Ω), horizontal plasma position (cm), total toroidal plasma current, SXR emission at $r=6$ cm low-field side (nA), total radiation from pyrobolometer (a.u.), visible bremsstrahlung ϵ_{VB} signal used for the Z_{eff} calculation (a.u.), line-averaged density from the interferometer (cm^{-3}).

shown in the next section, the AWCD drop in loop volts cannot be due to a change in inductance.

V. PLASMA TURN-OFF EXPERIMENTS

The plasma inductance (L) and resistance (R) was measured with a plasma termination experiment. For a series of nominally identical shots, Ohmic power supply and RF power are cut off, and the plasma column presumably dissipates on L/R time scales. Prior to the plasma termination, total plasma current I_p is clamped at a constant value by Ohmic and operator feedback, while the loop voltage is allowed to change from RF effects, as in Fig. 2. The circuit equation,

$$V_l = I_{\mathrm{Ohm}} R + L\,\frac{\partial I_{\mathrm{tot}}}{\partial t} + I_{\mathrm{tot}}\,\frac{\partial L}{\partial t}, \tag{9}$$

is solved before and after cutoff time, yielding two equations, and two unknowns (L,R). We assume that to lowest order $L^{(0)}$, $R^{(0)}$ do not change too much during the ± 1.5 ms

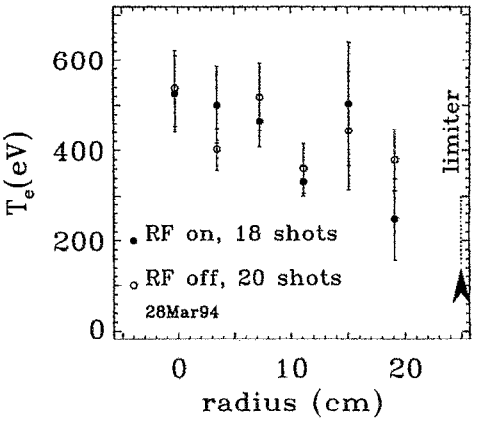

FIG. 3. Multipoint Thomson scattering electron temperature, measured in a vertical chord, averaged over 18 shots with RF (solid circles) and 20 (empty circles) without RF.

averaging window about the plasma cutoff time, where energy confinement time is approximately 4–6 ms. The lowest-order approximation for Ohmic current,

$$I_{\mathrm{Ohm}}^{(0)} = I_{\mathrm{tot}} - I_{\mathrm{CD}}, \tag{10}$$

is estimated to be proportional to the difference between AWCD reduced loop volts and the fitted loop volts, as seen in Fig. 5. We initially treat $I_{\mathrm{tot}}(\partial L/\partial t)$ as a small correction, and from a series of nominally identical shots calculate $L^{(0)}(t)$, $R^{(0)}(t)$ without it. From Eq. (9), we find the adjusted $I_{\mathrm{Ohm}}^{(1)}$ using $I_{\mathrm{tot}}(\partial L/\partial t)$, $L^{(0)}$, $R^{(0)}$, and recalculate $L^{(1)}(t)$, $R^{(1)}(t)$. The result shown in Fig. 6 is that $L^{(1)}(t)$ increases some 4%–8% over 40 ms during the RF pulse. Here $R^{(1)}(t)$ increases 40%–70% over this time interval, which is consistent with the Z_{eff}, ϵ_{VB} data, which is overlaid for comparison and corresponds to the increase in resistivity due to RF-induced impurity generation. The Ohmic $I_{\mathrm{Ohm}}^{(1)}$ decreases from 65 to 30–40 kA, corresponding to AWCD I_{CD}=25–35 kA during the entire RF pulse.

A check on $I_{\mathrm{tot}}(\partial L/\partial t)$ shows that it is approximately 0.1–0.25 V, which is smaller than the RF-induced change in loop volts, consistent with the initial presumption.

The total inductance of the toroidal current channel depends on the geometry and internal inductance l_i,

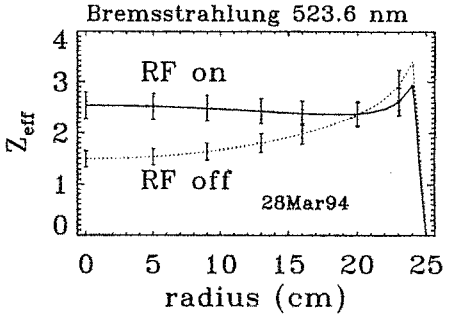

FIG. 4. Calculated Z_{eff} radial profile, Abel inverted from multiple chord measurements of ϵ_{VB}, as shown in Fig. 2, taken at times 10 ms before and after the start of RF.

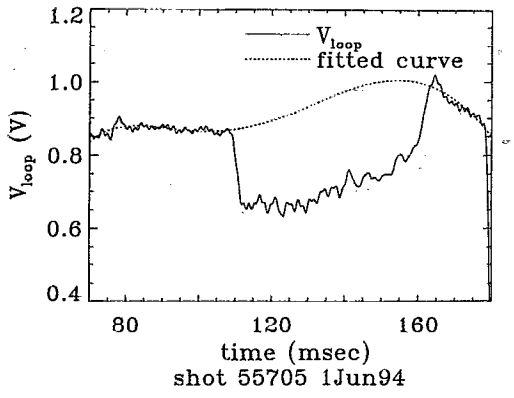

FIG. 5. Example shot showing a time record of loop voltage, with the curve fitted estimation of what V_{loop} would be with rising Z_{eff}, but no AWCD to depress the V_{loop}.

$$L=\mu_0 R_0[\ln(8R/a)-2+l_i/2]. \tag{11}$$

The measured $L(t)$ from Fig. 6 at plasma turn-off increases slowly, 4%–8%, during the RF pulse, which would inductively drive the loop voltage *up*, not down. The plasma radial position is held steady within 0.2%, so that the internal inductance,

$$l_i=\int_0^1 2\,\frac{B_\theta^2(\rho)}{B_\theta^2(1)}\,\rho\,d\rho, \tag{12}$$

must be affected by the RF. As the AWCD flux diffuses inward, the shape of I_p probably peaks slowly throughout the RF pulse, to account for the l_i integral that increases an estimated 20% with time.

VI. ESTIMATE FRACTION OF AWCD

We estimate the amount of current drive with a circuit model, using Spitzer resistivity for the Ohmic portion of the current. A uniform toroidal electric field is assumed from loop voltage,

$$E_z\approx\frac{V_l}{2\pi R_0}, \tag{13}$$

with a circuit model given by Eq. (9). Ohmic current I_{Ohm} driven by the measured loop volts decreases during RF pulse. For now, we neglect the small inductive corrections. Including them will increase our estimate of AWCD. From (9) we can estimate the fractional ratio of AWCD to total tokamak current as I_{CD}/I_{tot},

$$\frac{I_{CD}}{I_{no\ RF}}=1-\frac{V_l^{RF}}{V_l^{no\ RF}}\,\frac{R_{no\ RF}}{R_{RF}}, \tag{14}$$

where the plasma resistance $R\propto Z_{eff}/T_e^{3/2}$, so that the ratio

$$\frac{I_{CD}}{I_{no\ RF}}\approx 1-\frac{V_l^{RF}}{V_l^{no\ RF}}\,\frac{Z_{eff\ no\ RF}}{Z_{eff\ RF}}\,\frac{T_{e,RF}^{3/2}}{T_{e,no\ RF}^{3/2}}. \tag{15}$$

For T_e and $Z_{eff}\approx$const during RF, AWCD fraction would be

$$\frac{I_{CD}}{I_{no\ RF}}\approx 30\%-40\%, \tag{16}$$

corresponding to I_{CD}=20–25 kA. But the experimental ratio I_{CD}/P_{RF}, following from Eq. (16), was predicated on constant Z_{eff}, whereas Fig. 4 shows that it rises 40%, increasing the estimate $I_{CD}/I_{no\ RF}\approx$40%–60% corresponding to a maximum I_{CD}=30–40 kA, consistent with Fig. 6(d). We estimate a pessimistic engineering efficiency $(I_{CD}/P_{RF})^{eng}$ assuming 20±5 kA to 32±5 kA from Fig. 6 and assuming RF power input P_{RF} from Fig. 2. We estimate from LION,[53] a two-dimensional toroidal cold plasma code and a kinetic code ALFA[54] that 70%–85% of the P_{RF} gets past the edge to the plasma core and Alfvén resonance region, so that during the RF pulse the P_{RF} varies between $P_{RF}\approx$150–200 kW $\times(0.70-0.85)\approx$105 to 170 kW RF power coupled to the core plasma, yielding

$$(I_{CD}/P_{RF})^{eng}\approx 0.19\pm0.04\ \text{A/W}. \tag{17}$$

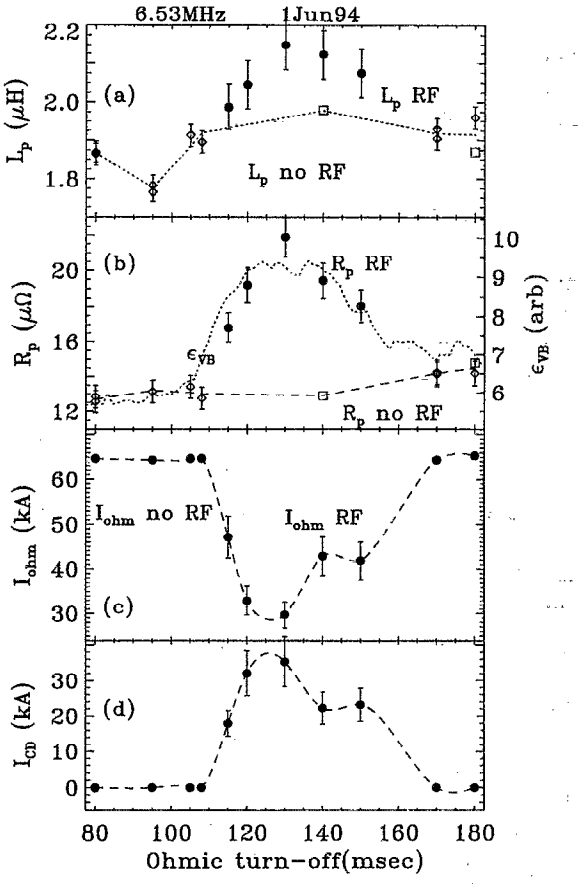

FIG. 6. (a) Plasma inductance L_p and (b) resistance R_p time evolution as inferred from a plasma termination experiment. Solid circles indicate data from times during RF pulse, open diamonds from other times for this shot series, and open squares are from similar shots with no RF during tokamak discharge. The curve fit to diamonds and squares corresponds to $L_p(t)$, $R_p(t)$ with no applied RF power. (b) Chord measurement at r=0 of ϵ_{VB}, scaled so ϵ_{VB} matches R_p before the RF pulse, agrees well with the inferred R_p, both in time evolution and magnitude. (c) Ohmic fraction and total I_p and (d) inferred time evolution of I_{CD} peaking at 35 kA from AWCD including the L_p, R_p data.

TABLE I. Comparison of Phaedrus-T experimental AWCD efficiency (both engineering and physics efficiencies) with CD experiments on other devices. The various acronyms have CD appended for Current Drive, where AW denotes the Alfvén Wave CD, LH denotes the Lower Hybrid CD, FW denotes the Fast (Magnetosonic) Wave CD, FW+LH denotes the synergistic Fast Wave+Lower Hybrid CD, ECCD denotes the Electron Cyclotron CD, and NB denotes the Neutral Beam CD experiments. We note that the conventional scaled parameter, $\gamma_{CD} = (I_{CD}/P_{RF})_{exp} n_e R_0$ favors larger denser machines than Phaedrus-T.

CD method	Experimental data	From theory $\tilde{\eta}_{CD}$		Standard scaled experimental
	$\left(\frac{I_{CD}}{P_{RF}}\right)_{exp\,t}$	$\left(\frac{I_{CD}}{P_{RF}}\right)_{theory} = \frac{1.9\times10^{19}}{2\pi R_0 \ln\Lambda}\frac{T_e}{n_e}\tilde{\eta}$		$\gamma_{CD}=\left(\frac{I_{CD}}{P_{RF}}\right)_{exp\,t} n_e R_0$
	(A/W)	(A/W)		$(A\,M^{-2}\,W^{-1})\times10^{19}$
AWCD engineering	0.19±0.04	Phaedrus-T	0.25–0.8	0.04±0.008
physics	0.27±0.05			0.06±0.01
LHCD[4]	0.2–1	PLT		0.5–3
FWCD[7]	0.11	D-IIID		0.09–0.12
FW+LHCD[6]	0.1–2	JET		2–4
ECCD[8]	0.06	T-10		0.15
NBCD[9]	0.08	DITE		0.2–0.3

We estimate from ALFA[54] that approximately 70% of the P_{RF} that gets past the edge resides in wave numbers that should contribute to AWCD, instead of electron heating. A more optimistic physics efficiency follows from reduced $P_{RF}\approx150$–200 kW$\times(0.70$–$0.85)\times0.7\approx75$ to 120 kW RF power coupled to the core plasma, yielding

$$(I_{CD}/P_{RF})^{phy}\approx0.27\pm0.05 \text{ A/W}. \tag{18}$$

This lower value of P_{RF} turns out to be consistent with the power balance arguments of the next section. The inductive $\partial L/\partial t$ term will increase this estimate further.

The usual calculations of efficiency[46,47] from Eqs. (6) and (7),

$$\frac{I_{CD}(A)}{P_{RF}(W)}\approx\frac{1.9\times10^{19}}{2\pi R_0 \ln\Lambda}\frac{T_e(keV)}{n_e(m^{-3})}\tilde{\eta}_{CD}, \tag{19}$$

where $\tilde{\eta}_{CD}\approx8$–$15$ and for $T_e\approx0.5\pm0.1$ keV yields the theoretical estimate of $I_{CD}/P_{RF}\approx0.25$–0.8 A/W for Phaedrus-T parameters, and a theoretically estimated physics figure of merit, $\gamma_{CD}^{th}=(I_{CD}/P_{RF})n_eR_0\approx0.55$–$1.7\times10^{18}$ A W^{-1} m^{-2}. In order to raise the conductivity enough to account for the AWCD data, i.e., the observed drop in V_{loop}, we would require a decrease in R, in spite of measured increase in Z_{eff} inferred from ϵ_{VB}. Therefore, the T_e would have to rise 35%–40%, significantly exceeding estimated errors in Thomson scattering T_e of $\approx\pm20\%$.

Table I shows a comparison of the current drive efficiency for the Phaedrus-I AWCD benchmarked against various other better known experiments. The experimental data in column 2 shows a favorable comparison with other CD scenarios, and $(I_{CD}/P_{RF})^{phy}$ overlaps the theoretical expectation. The experimental scaling from Eq. (8) most commonly used to compare CD efficiency is shown in column 3, and tends to favor larger and denser experiments than that of Fig. 2, where $\langle n_e\rangle=2.3\times10^{18}$ m^{-3}.

VII. POWER BALANCE

Even though the RF power input ($P_{RF}\approx160$–200 kW, 180 kW average) is three to four times the Ohmic power input ($P_{Ohm}\approx55$ kW before RF), measurements of the edge density and temperature, radiated power, or stored plasma particle energy do not account for the excess power input. Possibly some of the extra power is converted to poloidal field energy by the increase in plasma internal inductance that we show in Fig. 6. The edge temperature is observed to increase approximately 50% from 25 to 30–40 eV, requiring some 4–6 J. For the following discussion, we will neglect this edge energy deposition, and also note that we cannot experimentally distinguish between heating power and current drive power. The particle energy is

$$W_{nT}=\tfrac{3}{2}n(T_i+T_e)\times V\approx250 \text{ J}, \tag{20}$$

where V is the plasma volume, and the inductive energy increases with time,

$$W_{ind}=\frac{1}{2}LI^2+\frac{1}{2}\int_0^t I^2\frac{\partial L}{\partial t}\,dt\approx\frac{1}{2}I^2(L+\Delta L), \tag{21}$$

so that $\frac{1}{2}LI^2\approx4300$ J and the poloidal field energy far exceeds the particle energy, i.e., $W_{ind}\gg W_{nT}$. A 4%–8% increase in L leads increases inductive energy by 250 J, which is approximately equal to W_{nT}, corresponding to approximately 6 kW power input over 40 ms. RF power input is three to four times the Ohmic power input, but energy confinement degrades from L-mode scaling,

$$\tau_E\approx\tau_E^0/(1+P_{RF}/P_{Ohm})^{1/2}, \tag{22}$$

relative to Ohmic τ_E^0, so with additional RF power, τ_E(RF) decreases to 0.5–$0.7\tau_E^0$.

In order to maintain the degraded power balance, we would require approximately twice the previous Ohmic input power, $2\times P_{Ohm}$ (before RF)≈110 kW. The Ohmic input power during the RF pulse P_{Ohm} (during RF)≈20 kW is

estimated as the reduced Ohmic current from Fig. 6 times the loop voltage from Fig. 5. The RF power input P_{RF} is taken from Fig. 2, where we estimate from LION a two-dimensional toroidal cold plasma code[53] that 85% of the average P_{RF} is absorbed in the Alfvén resonance region. The P_{RF} peaks at $t=120-130$ ms, so for peak AWCD we take $P_{RF}=200$ kW $\times 0.85 \approx 170$ kW. Then power in minus the power out is estimated as

$$P_{RF}+P_{Ohm}\ [\text{during RF}]-2\times P_{Ohm}\ [\text{before RF}]$$
$$\approx 170\ \text{kW}+20\ \text{kW}-10\ \text{kW}\approx 80\ \text{kW}. \quad (23)$$

Almost half the RF power is unaccounted for. We speculate that the "extra" 80 kW of RF power is available to increase the poloidal field energy and inductance. This is consistent with the reduced $P_{RF}\approx 75-120$ kW available for AWCD we invoked for Eq. (18). The ratio of RF power converted poloidal field energy would then be approximately 6 kW/80 kW≈7.5%, corresponding to 3% of the total P_{RF}.

VIII. TIME SCALES

For this experiment, the short 5–10 ms experimental time scale for loop voltage drops is consistent with poloidal AWCD flux deposition near the edge. Fractional changes in the $I_p\approx$const current profile and inductive energy are small, so loop voltage changes can occur much faster than changes in the current profile. Changes in tokamak plasma current (in series with the Ohmic Power Supply) ought to occur on an inductive $L/2R\approx 70$ ms time scale. On the other hand, if the inductance increases, then the poloidal flux must diffuse inward much faster than resistive time scales,

$$\tau_R \approx \mu_0 a^2/\eta_R, \quad (24)$$

which are smaller on the edge because resistivity is high at the edge $\eta_R \approx Z_{\text{eff}} \ln(\Lambda)/T_e^{3/2}$. At lower densities, theory and code predictions[44,45] locate Alfvén resonances and continuum damping nearer the plasma edge than the core, near $r/a\approx 0.7$. At higher densities, theory and code predictions[44,45] locate Alfvén resonances in the plasma core, and hence more centrally localized AWCD.

IX. OPTIMAL WAVE NUMBER

Density scaling can be observed when the wave number is normalized to the ion skin depth c/ω_{pi}. In Fig. 7 we show the AWCD-induced change in loop voltage normalized to the loop voltage prior to the RF pulse plotted versus the dominant vacuum launch k_z component of the antenna. This appears to show an optimum wave number location, $k_z c/\omega_{pi}(r=0)\approx 1$, for this frequency, $\omega\approx 0.7\omega_{cH}$ $(r=0)$, on the Alfvén ion–ion hybrid dispersion relation.[17] These data suggest that for high-density operation, a compact antenna launching large k_z would be useful.

Larger k_z (smaller v_ϕ) might result in less FM wave access to the core because of the radial edge evanescence mentioned in Sec. II. On the other hand, one might increase density with ion mass, or exploit more extensive antenna arrays, or the radial upshift for inward propagating k_z,[51] or heavier ion species with lower Alfvén speeds and lower

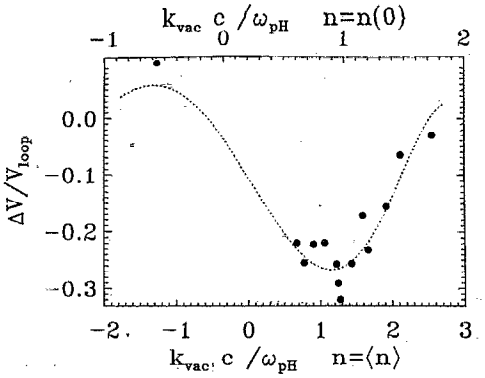

FIG. 7. Normalized drop in AWCD-induced loop voltage plotted against dominant vacuum spectrum wave number normalized to the ion skin depth $\kappa=k_z c/\omega_{pi}$, where the density and ion skin depth is calculated from averaged line density on the bottom scale, and estimated peak density on the top scale.

v_ϕ/v_e (e.g., D, He^3, T) or Alfvén ion–ion hybrid[18,55] scenarios to gain access to AWCD regimes more efficient than shown here.

X. CONCLUSION

We have shown the first experimental evidence of AWCD in a tokamak. We estimate a minimum of 20 kA to a peak 32 kA±5 kA out of 65 kA total current, or 30%–55% of the total has been driven. The experimental estimate for efficiency depends strongly on what fractions of the launched RF power P_{RF} we assume are coupled to AWCD and electron heating. For peak AWCD the engineering efficiency is calculated from the inferred current drive and total P_{RF} applied $(I_{CD}/P_{RF})^{\text{eng}}\approx 0.19\pm 0.04$ A/W. The physics efficiency $(I_{CD}/P_{RF})^{\text{phy}}\approx 0.27\pm 0.05$ A/W follows from the smaller estimated P_{RF} fraction that is coupled to AWCD.

The predicted $I_{CD}/P_{RF}\approx 0.25-0.8$ A/W for a $Z_{\text{eff}}\approx 2-3$ is slightly above $(I_{CD}/P_{RF})^{\text{eng}}$, overlaps our physics estimate $(I_{CD}/P_{RF})^{\text{phy}}$, and is consistent with a smaller estimate of coupled P_{RF} and our inability to distinguish between heating and CD P_{RF}. The significant 30%–40% drop in loop voltage we observe cannot be explained by any plausible increase in T_e, or decrease in inductive plasma energy W_{ind}, or the associated inductive loop voltage corrections $L\partial I_p/\partial t$ or $I_p(\partial L/\partial t)$, or changes in Z_{eff}.

Independently measured V_{loop}, T_e, Z_{eff}, and calculated L, R are all consistent with this conclusion.

The bootstrap current fraction for the tokamak discharges, such as shown in Fig. 2 is, at most, a very small fraction of the noninductive current driven. We estimate[56] it as

$$I_{BS}/I_{tot}\approx 0.67\beta_p\epsilon^{1/2}\leqslant 2\%, \quad (25)$$

where the inverse aspect ratio $\epsilon=a/R_0$ and the poloidal beta $\beta_p\leqslant 0.1$.

Low phase speed CD is attractive because less power is required to push a slow electron than a fast one, and these waves resonate near v_e and Landau damp on the large bulk electron population. AWCD has the potential to provide spa-

tially tunable noninductive current profiles, tailoring profiles of plasma current I_p, and electron temperature T_e, with no high-density limit, which is an advantage over LHCD. In fact, high density would be an advantage, because of the consequent low Alfvén speed, and hence low v_ϕ/v_e and high efficiency. In a low aspect ratio tokamak, where the densities are high and the toroidal B field is low, the low v_A is especially attractive, and investigations of whether trapping is an issue would be crucial.

Several issues are left for future investigations. We hope to reduce the value of Z_{eff} to increase the CD efficiency, as seen from the calculations of Ehst–Karney and shown in Fig. 1. This would probably be more effective than merely adding more RF power. Some experimental evaluation of the validity of the electron trapping arguments needs to be carried out, because these objections, if valid, could severely restrict the usefulness of AWCD. On the other hand, to gain access to AWCD regimes more efficient than shown here, one might exploit more extensive antenna arrays, or the radial upshift for inward propagating k_z,[51] or heavier ion species with lower Alfvén speeds and lower v_ϕ/v_e (e.g., D, He^3, or T), or Alfvén ion–ion hybrid[18,55] scenarios.

ACKNOWLEDGMENT

This work was supported by U.S. Department of Energy Grant No. DE-FG02-8853264.

[1]N. Fisch, Rev. Mod. Phys. **59**, 175 (1987).
[2]T. Yamamoto, T. Imai, M. Shimada, N. Suzuki, M. Maeno, S. Konoshima, T. Fujii, K. Uehara, T. Nagashima, A. Funahashi, and N. Fujisawa, Phys. Rev. Lett. **45**, 716 (1980).
[3]S. Luckhardt, M. Porkolab, S. Knowlton, K-I. Chen, A. Fisher, F. Mcdermott, and M. Mayberry, Phys. Rev. Lett. **48**, 152 (1982).
[4]S. Bernabei, C. Daghney, P. Efthimion, W. Hooke, J. Hosea, F. Jobes, A. Martin, E. Mazzucato, E. Meservey, J. Stevens, S. Von Goeler, and R. Wilson, Phys. Rev. Lett. **49**, 1255 (1982).
[5]F. Jobeš, J. Stevens, R. Bell, S. Bernabei, A. Cavallo, T. Chu, S. Cohen, B. Denne, P. Efthimion, E. Hinnov, W. Hooke, J. Hosea, E. Mazzucato, R. McWilliams, R. Motley, S. Suckewer, G. Taylor, J. Timberlake, S. Von Goeler, and R. Wilson, Phys. Rev. Lett. **52**, 1005 (1984).
[6]J. Jacquinot, V. Bhatnagar, C. Gormezzano, and the JET team, Plasma Phys. Controlled Fusion A **35**, 35 (1993).
[7]R. I. Pinsker, F. W. Baitty, S. C. Chiu, J. S. DeGrassie, C. B. Forest, R. H. Goulding, D. J. Hoffman, H. Ikezi, Y. R. Lin-Liu, T. C. Luce, C. C. Petty, M. Porkolab, R. Prater, J. P. Squire, D. W. Swain, and the DIII-D group, *Recent Results from Fast Wave Current Drive Experiments on DIII-D*, Proceedings of the 21st European Physical Society Conference on Controlled Fusion and Plasma Physics, Montpelier, 27 June–1 July 1994, edited by E. Joffrin, P. Platz, and P. E. Stott (European Physical Society, Petit-Lancy, Switzerland, 1994), Vol. III, p. 1118.
[8]V. V. Alikaev, A. A. Bagdasarov, A. A. Borshchegovskij, V. V. Chistyakov, M. M. Dremin, Yu. A. Gorelov, Yu. V. Esipchuk, D. B. Evdokimov, D. A. Kislov, V. A. Krupin, S. E. Lysenko, G. E. Notkin, Yu. D. Pavlov, K. A. Razumova, I. N. Roi, A. N. Sushkov, P. V. Savrukhin, V. M. Trukhin, N. L. Vasin, V. A. Vershkov, C. Forest, and J. Lohr, in Ref. 7, p. 1057.
[9]J. Wesson, *Tokamaks* (Clarendon, Oxford, 1987), p. 80.
[10]J. Tataronis and W. Grossman, Z. Phys. **261**, 203 (1973).
[11]L. Chen and A. Hasegawa, Phys. Fluids **17**, 1399 (1974).
[12]D. W. Ross, G. L. Chen, and S. W. Mahajan, Phys. Fluids **25**, 652 (1982).
[13]J. M. Davila, Astron. Astrophys. **317**, 514 (1987).
[14]R. L. Lysak and C. T. Dum, J. Geophys. Res. **88**, 365 (1983).
[15]A. Hasegawa and L. Chen, Phys. Fluids **19**, 1924 (1976).
[16]R. Majeski, P. Probert, P. Moroz, T. Intrator, R. Breun, D. Brouchous, H. Y. Che, J. R. DeKock, D. Diebold, M. Doczy, R. Fonck, N. Hershkowitz, R. D. Johnson, M. Kishinevsky, G. McKee, J. Meyer, P. Nonn, S. P. Oliva, J. Pew, J. Sorenson, T. Tanaka, M. Vukovic, and G. Winz, Phys. Fluids B **5**, 2506 (1993).
[17]G. A. Collins, F. Hoffman, B. Joye, R. Keller, A. Lietti, J. B. Lister, and A. Pochelon, Phys. Fluids **29**, 2260 (1986).
[18]T. Intrator, P. Probert, M. Vukovic, A. Elfimov, R. Durst, S. Wukitch, M. Cekic, R. Breun, D. Brouchous, D. Diebold, M. Doczy, D. Edgell, R. Fonck, N. Hershkowitz, M. Kishinevsky, R. Majeski, C. Litwin, G. McKee, and G. Winz, "Alfven ion–ion hybrid heating in the Phaedrus-T tokamak," submitted to Phys. Rev. Lett.
[19]S. Wukitch, M. Vukovic, R. Breun, D. Brouchous, D. Diebold, M. Doczy, D. Edgell, A. Elfimov, N. Hershkowitz, T. Intrator, M. Kishinevsky, C. Litwin, P. Moroz, and P. Probert, Phys. Rev. Lett. **74**, 2240 (1995).
[20]B. Joye, A. Lietti, J. B. Lister, J. M. Moret, and W. Simm, Phys. Rev. Lett. **56**, 2481 (1986).
[21]A. B. Murphy, Nucl. Fusion **31**, 465 (1991).
[22]R. Cross, Plasma Phys. **25**, 1377 (1983).
[23]F. D. Witherspoon, S. C. Prager, and J. C. Sprott, Phys. Rev. Lett. **53**, 1559 (1984).
[24]H. Weisen, K. Appert, G. G. Borg, B. Joye, A. J. Knight, J. B. Lister, and J. Vaclavik, Phys. Rev. Lett. **63**, 2476 (1989).
[25]R. A. Demirkhanov, A. G. Kirov, G. I. Stapenko, S. E. Il'inskij, Eh. M. Lomakin, V. V. Onischenko, L. F. Ruchko, A. V. Sukhachev, V. V. Medun, and N. I. Malykh, *Plasma Physics and Controlled Fusion Research*, 9th Conference Proceedings, Baltimore, 1–8 September 1982 (International Atomic Energy Agency, Vienna, 1983), Paper IAEA-CN-41/J-1-2, Vol. 2, p. 91.
[26]V. P. Bhatnagar, J. Jacquinot, and the JET Team, "Fast wave heating and current drive scenarios for JET and ITER," JET-P(94)23, submitted to Fusion Eng. Design
[27]R. J. Bickerton, Comments Plasma Phys. Controlled Fusion **1**, 95 (1972).
[28]N. Fisch and C. Karney, Phys. Fluids **24**, 27 (1981).
[29]S. Puri and R. Wilhelm, *Proceedings of the 8th Topical Conference on Radio Frequency Power in Plasmas*, Irvine, 1989, AIP Conf. Proc. 190, edited by R. McWilliams (American Institute of Physics, New York, 1989), p. 458.
[30]J. Vaclavik and K. Appert, Nucl. Fusion, **31**, 1945 (1991).
[31]R. Majeski, P. Probert, T. Tanaka, D. Diebold, R. Breun, M. Doczy, R. Fonck, N. Hershkowitz, T. Intrator, G. McKee, P. Nonn, J. Pew, and J. Sorenson, Fusion Eng. Design **24**, 159 (1994).
[32]R. C. Cross, *An Introduction to Alfvén Waves* (Hilger, Bristol, UK, 1988).
[33]S. N. Golovato and J. Shohet, Phys. Rev. Lett. **37**, 1272 (1976).
[34]T. Obiki, T. Mutoh, S. Adachi, A. Sasaki, A. Iiyoshi, and K. Uo, Phys. Rev. Lett. **39**, 812 (1977).
[35]A. G. Kirov, A. Elfimov, D. Vojtenko, A. Sukachev, M. Stotland, S. Lozovskij, and V. Dorokhov, *Plasma Physics and Controlled Fusion Research*, 14th Conference Proceedings, Washington, DC, 1–6 October 1990 (International Atomic Energy Agency, Vienna, 1991), Paper IAEA-CN-53/E-III-13, Vol. 1, p. 831.
[36]T. Evans, P. Valanju, J. Benesch, R. Bengston, Y. Li, S. Mahajan, M. Oakes, S. Ross, X. Wang, and J. Watkins, Phys. Rev. Lett. **53**, 1743 (1984).
[37]W. Gekelman, D. Leneman, J. Maggs, and S. Vincena, Phys. Plasmas **1**, 3775 (1994).
[38]Y. Amagishi, IEEE Trans. Plasma Sci. **PS-20**, 622 (1992).
[39]M. Cekic, B. A. Nelson, F. Ribe, Phys. Fluids B **4**, 392 (1992).
[40]D. Roberts, N. Hershklowitz, and J. Tataronis, Phys. Fluids B **2**, 787 (1990).
[41]M. Inutake, M. Ichimura, H. Hojo, Y. Kimura, R. Katsumata, S. Adachi, Y. Nakashima, A. Itakura, A. Mase, and S. Miyoshi, Phys. Rev. Lett. **65**, 3397 (1990).
[42]R. A. Breun, D. Brouchous, D. Diebold, R. Fonck, N. Hershkowitz, T. Intrator, Y. J. Kim, M. Kishinevsky, W. Li, R. Majeski, J. Pew, P. Probert, E. Y. Wang, Y. Wen, H. Che, M. Doczy, G. McKee, J. Sorenson, T. Tanaka, M. Vukovic, P. Bellan, and M. R. Brown, Fusion Technol. **19**, 1327 (1991).
[43]J. Winter, H. G. Esser, and H. Reimer, J. Nucl. Mat. **176&177**, 486 (1990).
[44]A. Hasegawa and C. Uberoi, *The Alfvén Wave*, Technical Information Center (U.S. Department of Energy, Washington, DC, 1982).
[45]A. Elfimov, J. Tataronis, and N. Hershkowitz, Phys. Plasmas **1**, 2637 (1994).
[46]See National Technical Information Service Document No. DE-85005427 (N. Uckan, "Noninductive drive in tokamaks," ORNL/TM-9296, 1985). Copies may be ordered from the National Technical Information Service, 5285 Fort Royal Road, Springfield, VA 22161.
[47]D. W. Faulconer, Trans. Fusion Technol. **25**, 188 (1994).

[48]D. Ehst and C. Karney, Nucl. Fusion **31**, 1933 (1991).
[49]D. J. Wort, Plasma Phys. **13**, 258 (1971).
[50]A. Elfimov and S. Puri, Nucl. Fusion **30**, 1251 (1990).
[51]H. Ikezi and R. Pinsker, Bull Am. Phys. Soc. **38**, 2068 (1993).
[52]I. H. Hutchinson, *Principles of Plasma Diagnostics* (Cambridge University Press, Cambridge, 1990), p. 175.
[53]L. Villard, K. Appert, R. Gruber, J. Vaclavik, Comput. Phys. Rep. **4**, 95 (1986).
[54]N. Hershkowitz, P. Moroz, P. Probert, T. Intrator, E. Y. Wang, D. Diebold, R. Breun, D. Brouchous, M. Doczy, D. Edgell, A. Elfimov, R. Fonck, M. Kishinevsky, C. Litwin, P. Nonn, S. Regan, M. Vukovic, J. Sorensen, J. Tataronis, M. Vukovic, X. Wang, and S. Wukitch, "Alfvén wave current drive and heating," to appear in *Plasma Physics and Controlled Fusion Research*, 15th Conference Proceedings, Seville, 26 September–1 October 1994 (International Atomic Energy Agency, Vienna, in press), Paper IAEA-CN-60/A3/5-P-10.
[55]R. Majeski, C. K. Phillips, and R. Wilson, Phys. Rev. Lett. **73**, 2204 (1994).
[56]B. B. Kadomtsev, *Tokamak Plasma: A Complex Physical System* (Institute of Physics, Philadelphia, PA, 1992), p. 131.